Study of the Line Optical Tweezers Characteristics Using a Novel Method and Establishing a Model for Cell Sorting

2009 Jpn. J. Appl. Phys. 48 072502

(http://iopscience.iop.org/1347-4065/48/7R/072502)

Study of the Line Optical Tweezers Characteristics Using a Novel Method and Establishing a Model for Cell Sorting

Ho-Chien Lin* and Long Hsu

Institute and Department of Electrophysics, National Chiao-Tung University, 1001 Ta Hsueh Road, Hsinchu, Taiwan 30010, R.O.C.

Received December 30, 2008; accepted April 13, 2009; published online July 21, 2009

Optical tweezers have become a powerful tool in cellular and molecule biology. Line optical tweezers enhanced its function in cell sorting. This study presents the line trap model, based on the ray-optics model, and demonstrates its accuracy for the line optical tweezers. The line optical tweezers system is established to produce the optical intensity distribution of a line pattern and to trap the micro-sized beads. The main parameter, optical intensity distribution, is used to calculate the trapping force distribution in the model. The two forces, trapping force and water dragging force, and the equation of motion is used to simulate the trajectory of micro-sized beads as they pass through the line pattern in flowing water in the microchannel. The trajectory is analyzed to determine the effective separation distance between the micro-sized beads or cells. The method will be applied in biological and medical detection.

DOI: 10.1143/JJAP.48.072502

1. Introduction

The miniaturization of cell separation techniques is a much-sought breakthrough in the development of the microfluidic lab-on-a-chip. Currently available standard cell sorting and screening systems involve flow cytometry and a microchannel chip, both of which have several limitations. Following many trials, the combination of the non-mechanical optical manipulation of optical tweezers and the microfluidic lab-on-a-chip may provide a new solution.

The cell sorting apparatus most frequently utilized today exploits optical and electronic detection associated with flow cytometry to detect specific cells rapidly. However, the large-sized and expensive flow cytometry is a drawback. In contrast, a microchannel chip is miniature and inexpensive. It exploits the characteristics of the microchannel chip to guide and differentiate among cells of different sizes. It comprises the microstructure and the dielectrophoresis (DEP). Although a microchannel chip is a tool of cell sorting, it has some limitations. First, the procedure is only applicable to fixed-sized cells and cannot be extended to apply to individual sample cells. Once the size, location and pattern of the structure fabricated on the chip have been set, neither the microstructure nor the electrode on the chip can be altered, despite the consistency between the cell and the sample cell size. Next, the electrode plates are normally placed at the bottom of the microchannel because an effective trapping domain of an electrode is only around 100 μm wide; therefore, a microchannel with a deeper domain is ineffective. Because of these unsolved problems, a microchannel chip has not been extensively applied.

Unlike a microchannel chip, optical tweezers perform not mechanical but optical trapping. They do not raise the difficulties of the microchannel encounters. Optical tweezers are a photonic device that exploits a focused laser beam to provide a trapping force. They function like a "hand" with which to trap and manipulate single cells or molecules under the microscope. Although an optical tweezers trap the micro-sized bead which effective trapping domain is only around 100 μm long, similar to that of a microchannel chip, the trapping point can be freely controlled in a microchannel of a large area. This feature enables trapped cells to be guided in the microchannel. The advantages of optical tweezers somewhat eliminate the limitations and drawbacks of microchannel chips. With a combination of microfluidic lab-on-a-chip, optical tweezers have been established to be powerful tools in the miniaturization of cell separation techniques.

This study proposes the model and the line optical tweezers system in which cells of various sizes are effectively separated in a microchannel. Since their invention by Ashkin *et al.*,[1] optical tweezers have opened up new areas of the study in cellular and molecular biology, because their ability to trap and manipulate single cells or molecules.[2–7] Reicherter and Curtis further constructed a system of holographic optical tweezers (HOT) by combining the programmable phase modulator (PPM) with traditional optical tweezers.[8,9] The HOT system enables many particles or cells to be manipulated simultaneously. Restated, it extends the application of optical tweezers from the generation of one trap to the generation of multiple traps simultaneously.[10] Based on HOT and the PPM, Tseng developed the line trap by arranging multiple traps in a line.[11] He also introduced the possibility of guiding and separating differently sized particles using the line trap. Grier focused on the relationship between phase modulation and optical intensity distribution of holographic line traps.[12,13] This work presents the line trap model and demonstrates its accuracy. The model is utilized to analyze the functions of line optical tweezers, including trapping, guiding and separation. The micro-sized bead/cell separation was determined as a function of velocity of flowing water and the included angle between the line pattern and direction of flow.

2. Model

This section proposes model of a line optical tweezers and experimentally demonstrates the accuracy of the model. The model was used to calculate the distribution of the trapping force when the micro-sized bead was trapped in the line optical tweezers for all of the line patterns produced by the PPM. Next, numerical simulation was used to calculate the trajectories of two micro-sized beads of different sizes under the influence of the different resultant forces that comprise the water dragging force and the trapping force. From the trajectories, the separation distance Δd of the two micro-

*E-mail address: hclin.ep89g@nctu.edu.tw

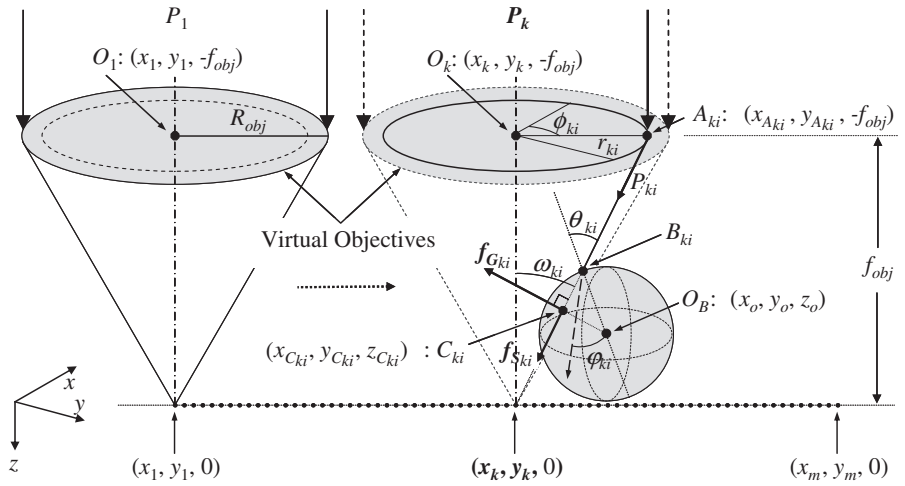

Fig. 1. A schematic drawing of the interaction between the line optical tweezers and the micro-sized bead. The line pattern at $z = 0$ which comprises m individual trapping points. Each trapping point corresponds to one-trap optical tweezers. The scattering force f_{Gki} and the gradient force f_{Ski} exerted by each one-trap optical tweezers on the micro-sized bead was calculated.

sized beads was calculated. Based on the model, this distance was used to determine the separation efficiency. Finally, the separation conditions of water flowing velocity v_w and included angle θ_w between the line pattern and direction of flow were determined.

To calculate the trapping force distribution of the trapped micro-sized beads, the interaction of the micro-sized beads immersed in an aqueous solution with line optical tweezers was considered. The five known parameters were the refractive index of the aqueous solution n_s, the refractive index of a micro-sized bead n_B, the radius R_B of the beads, the mass M of the beads, and the laser wavelength λ. The center of the trapped micro-sized bead was designated the origin O_B with coordinats (x_o, y_o, z_o), the length of the line pattern was L and the total laser power of the line pattern was P. This model assumes that the line pattern is formed from many individual trapping points. Then, based on Ashkin's Single Trap Ray-Optics model, the trapping force distribution at each trapping point is individually calculated and then summed to determine the trapping force distribution of the line-trap model.

Figure 1 shows the line pattern at $z = 0$ which comprises m individual trapping points is established first. The coordinate of each trapping point k is $(x_k, y_k, 0)$, where $1 \le k \le m$. Next, each trapping point is assumed to have a laser power P_k that differs from each of the others, for a total power ($P = \sum_{k=1}^{m} P_k$). Additionally, since each trapping point corresponds to one-trap optical tweezers, on a simulated objective can be assumed to be located on the top of each trapping point. Each laser power P_k is that of a parallel incident laser beam. When all the corresponding incident laser beams converge, they meet at focal points in the focal plane, which later become a line pattern. The specification of these virtual objectives is assumed to be identical to that of the experimental objectives. The focus is defined as f_{obj} and the radius of the entrance pupil is R_{obj}. Accordingly, the coordinate of any center of the objectives is O_k, with coordinate $(x_k, y_k, -f_{obj})$. To simulate the focusing of a laser beam, each beam is divided into j rays, for convenience of tracing. Since each trapping point corresponds to its own laser beam, the laser power of any ray i at any trapping point k is $P_{ki} = P_k/j$, where $1 \le i \le j$.

In ray tracing, on the objective of a virtual microscope, the i-th ray of the k-th laser beam was assumed to be emitted at an angle of inclination ω_{ki} from point A_{ki}, with coordinate $(x_{A_{ki}}, y_{A_{ki}}, -f_{obj})$ to one of the points B_{ki}, on the surface of the micro-sized bead, and then to refract into the bead. Geometry is used to obtain the coordinate of B_{ki} and the coordinate of the incident ray that is closest to the center of the bead, C_{ki} $(x_{C_{ki}}, y_{C_{ki}}, z_{C_{ki}})$.

$$x_{C_{ki}} = \frac{x_o + y_o \cdot \tan\varphi_{ki} - \dfrac{z_o}{\tan\Omega_{ki} \cdot \cos\varphi_{ki}}}{1 + \tan^2\varphi_{ki} + \left(\dfrac{1}{\tan\Omega_{ki} \cdot \cos\varphi_{ki}}\right)^2}, \quad (1)$$

$$y_{C_{ki}} = y_k + (x_{C_{ki}} - x_k) \cdot \tan\varphi_{ki}, \quad (2)$$

and

$$z_{C_{ki}} = \frac{-(x_{C_{ki}} - x_k)}{\tan\Omega_{ki} \cdot \cos\varphi_{ki}}, \quad (3)$$

which

$$\varphi_{ki} = \tan^{-1}\left(\frac{y_{A_{ki}} - y_k}{x_{A_{ki}} - x_k}\right), \quad (4)$$

is the angle between x-axis and vector O_k to vector A_{ki},

$$\omega_{ki} = \tan^{-1}\left(\frac{r_{ki}}{f_{obj}}\right), \quad (5)$$

and

$$r_{ki} = \sqrt{(x_{A_{ki}} - x_k)^2 + (y_{A_{ki}} - y_k)^2}, \quad (6)$$

is the distance between A_{ki} to O_k; accordingly, the incident angle θ_{ki} and the refraction angle φ_{ki} at point B_{ki} for this ray can be obtained:

$$\theta_{ki} = \sin^{-1}\frac{\sqrt{(x_o - x_{C_{ki}})^2 + (y_o - y_{C_{ki}})^2 + (z_o - z_{C_{ki}})^2}}{R_B}, \quad (7)$$

$$\varphi_{ki} = \sin^{-1}\left(\frac{n_s \cdot \sin\theta_{ki}}{n_B}\right). \quad (8)$$

Consider both s- and p-polarizations under the influence of electric field; the ray in position B_{ki}, the reflectance R_{ki} and transmittance T_{ki} can be expressed as

$$R_{ki} = \begin{cases} \left(\dfrac{n_s \cdot \cos\theta_{ki} - n_B \cdot \cos\varphi_{ki}}{n_s \cdot \cos\theta_{ki} + n_B \cdot \cos\varphi_{ki}}\right)^2 & \text{for s-polorization} \\ \left(\dfrac{n_s \cdot \cos\varphi_{ki} - n_B \cdot \cos\theta_{ki}}{n_s \cdot \cos\varphi_{ki} + n_B \cdot \cos\theta_{ki}}\right)^2 & \text{for p-polorization} \end{cases}, \quad (9)$$

and

$$T_{ki} = \begin{cases} \left(\dfrac{n_B \cdot \cos\varphi_{ki}}{n_s \cdot \cos\theta_{ki}}\right)\left(\dfrac{2n_s \cdot \cos\theta_{ki}}{n_s \cdot \cos\theta_{ki} + n_B \cdot \cos\varphi_{ki}}\right)^2 & \text{for s-polorization} \\ \left(\dfrac{n_B \cdot \cos\varphi_{ki}}{n_s \cdot \cos\theta_{ki}}\right)\left(\dfrac{2n_s \cdot \cos\varphi_{ki}}{n_s \cdot \cos\varphi_{ki} + n_B \cdot \cos\theta_{ki}}\right)^2 & \text{for p-polorization} \end{cases}. \quad (10)$$

According to Ashkin's RO model, each incident ray that passes through the micro-sized bead exerts two main forces that are mutually perpendicular: one is a scattering force, which acts parallel to the incident ray, and the other is gradient force, which acts perpendicular to the incident ray.[14,15] The method of the RO model is then applied to the line trap model. As shown in Fig. 1, when the i-th ray of the k-th laser beam passes through the micro-sized bead, the exerted scattering force $f_{S_{ki}}$ and gradient force $f_{G_{ki}}$ can be expressed as

$$f_{S_{ki}} = \frac{n_s \cdot P_{ki}}{c}\left\{1 + R_{ki} \cdot \cos 2\theta_{ki} - \frac{T_{ki}^2[\sin(2\theta_{ki} - 2\varphi_{ki}) + R_{ki} \cdot \cos 2\theta_{ki}]}{1 + R_{ki}^2 + 2R_{ki} \cdot \cos 2\varphi_{ki}}\right\}, \quad (11)$$

and

$$f_{G_{ki}} = \frac{n_s \cdot P_{ki}}{c}\left\{R_{ki} \cdot \sin 2\theta_{ki} - \frac{T_{ki}^2[\sin(2\theta_{ki} - 2\varphi_{ki}) + R_{ki} \cdot \sin 2\theta_{ki}]}{1 + R_{ki}^2 + 2R_{ki} \cdot \cos 2\varphi_{ki}}\right\}, \quad (12)$$

where c is velocity of light in vacuum.

To calculate the resultant forces associated with the total number of incident rays on the micro-sized bead, the resultant forces, scattering force and gradient force, are first converted into three resultant force components along the xyz-axes:

$$f_{x_{ki}} = -\frac{r_{ki} \cdot \cos\varphi_{ki}}{\sqrt{{r_{ki}}^2 + {f_{obj}}^2}} f_{S_{ki}} - \frac{f_{obj} \cdot \cos\varphi_{ki}}{\sqrt{{r_{ki}}^2 + {f_{obj}}^2}} f_{G_{ki}}, \quad (13)$$

$$f_{y_{ki}} = -\frac{r_{ki} \cdot \sin\varphi_{ki}}{\sqrt{{r_{ki}}^2 + {f_{obj}}^2}} f_{S_{ki}} - \frac{f_{obj} \cdot \sin\varphi_{ki}}{\sqrt{{r_{ki}}^2 + {f_{obj}}^2}} f_{G_{ki}}, \quad (14)$$

and

$$f_{z_{ki}} = \frac{f_{obj}}{\sqrt{{r_{ki}}^2 + {f_{obj}}^2}} f_{S_{ki}} - \frac{r_{ki}}{\sqrt{{r_{ki}}^2 + {f_{obj}}^2}} f_{G_{ki}}. \quad (15)$$

Adding all of the components of the trapping force exerted by each ray on the micro-sized bead at all of the trapping points, yields the components of each axial trapping force $\boldsymbol{F}_{Line}$ in the line trap:

$$F_{Line,x}(x_o, y_o, z_o) = \sum_{k=1}^{m}\left(\sum_{i=1}^{j} f_{x_{ki}}\right), \quad (16)$$

$$F_{Line,y}(x_o, y_o, z_o) = \sum_{k=1}^{m}\left(\sum_{i=1}^{j} f_{y_{ki}}\right), \quad (17)$$

and

$$F_{Line,z}(x_o, y_o, z_o) = \sum_{k=1}^{m}\left(\sum_{i=1}^{j} f_{z_{ki}}\right), \quad (18)$$

where (x_o, y_o, z_o) is the center position of the micro-sized bead, m is the total number of trapping points, and j is the total number of rays on a trapping point, respectively. After the trapping force distribution where the line trap was used to hold on the micro-sized bead was determined, the trajectory of the micro-sized bead was simulated using its motion equation. Given the velocity of the flowing water, $\boldsymbol{v}_w$ and the line trap in the microchannel, two forces, the water dragging force $\boldsymbol{F}_d$ and the trapping force $\boldsymbol{F}_{Line}(x_o, y_o, z_o)$ are expected to act on the micro-sized bead simultaneously. These two forces and the equation of motion of the trapped micro-sized bead are

$$M\frac{d^2\boldsymbol{r}}{dt^2} = \boldsymbol{F}_d(\boldsymbol{r}) + \boldsymbol{F}_{Line}(\boldsymbol{r}), \quad (19)$$

where M denotes the mass of a micro-sized bead, $\boldsymbol{r} = r(x_o, y_o, z_o)$ is the vector of the center of the micro-sized bead, and t is time. Here the water dragging force $\boldsymbol{F}_d$ is

$$\boldsymbol{F}_d(\boldsymbol{r}) = -6\pi\eta R_B\left(\boldsymbol{v}_w - \frac{d\boldsymbol{r}}{dt}\right), \quad (20)$$

where η is the fluid viscosity, and R_B is the radius of the micro-sized bead. Based on the assumption that the micro-sized bead reaches its terminal velocity, its acceleration will be zero. Therefore, eq. (19) is modified to

$$\frac{d\boldsymbol{r}}{dt} = \boldsymbol{v}_w - \frac{\boldsymbol{F}_{Line}(\boldsymbol{r})}{6\pi\eta R_B}. \quad (21)$$

Next, the finite-difference time-domain (FDTD)[16] and eq. (21), adopted to carry out a numerical analysis and obtain the trajectory $\boldsymbol{r}(t)$ of the micro-sized bead under the influence of the water dragging force $\boldsymbol{F}_d$ and the trapping force $\boldsymbol{F}_{Line}$ in the line pattern. Equation (21) can be rewritten as following based on the FDTD;

$$\Delta\boldsymbol{r}_n = \left[\boldsymbol{v}_w - \frac{\boldsymbol{F}_{Line}(\boldsymbol{r}_n)}{6\pi\eta R_B}\right]\Delta t, \quad (22)$$

where $\Delta\boldsymbol{r}_n = \boldsymbol{r}_n - \boldsymbol{r}_{n-1}$ is the change in position of a moving micro-sized bead by unit time Δt. Equation (22) yields the trajectory of any each micro-sized bead in the line pattern with various included angles.

The trajectories of two beads of different sizes and the difference between the vertical distances d_1 and d_2 associated with the oblique displacements are compared. This difference is the separation ($\Delta d = d_1 - d_2$) of the two beads in the line trap, and is used to determine separation efficiency. The water flow velocity v_w and the included angle θ_w between the line pattern and the flowing direction are separation condition.

3. Experimental Procedure

3.1 Setup

The line optical tweezers system that is used in this

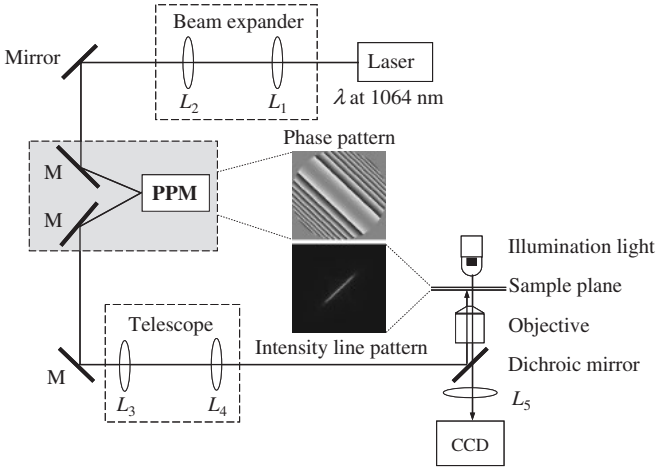

Fig. 2. A schematic diagram of the line optical tweezers setup: a traditional optical tweezers apparatus and the PPM.

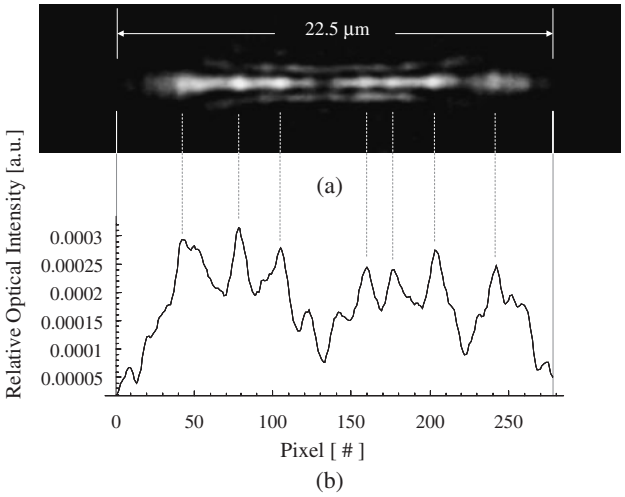

Fig. 3. (a) 2D image of a line pattern and (b) its equivalent 1D optical intensity distribution.

experiment are those used in the HOT system. Basically, they comprise a traditional single trap optical tweezers apparatus and an inserted reflection PPM (Hamamatsu X8267), as displayed in Fig. 2. Notably, the PPM should be inserted in the equivalent front focal plane of the microscope, such that the modulated phase pattern, adjusted by PPM, can generate a line pattern via a Fourier transform in the rear focal sample plane of the microscope.

To utilize fully the phase-modulation of a laser beam by PPM, a two-lens (L_1 and L_2) laser beam expander is adapted to extend the cross-sectional area of a diode laser beam (λ at 1064 nm) to fill the receiving area of the PPM. After the modulated laser beam has been refracted, it passes through the two lenses of the telescope (L_3 and L_4) to reduce cross-sectional area of a laser beam to fill the entrance pupil of the objectives. Then, the narrowed laser beam passes through a dichroic mirror into the objective (Olympus 100X, numerical aperture = 1.25, oil), producing a line pattern in the sample plane. The sample plane was moved by manipulating the actuator. To observe the experiment and analyze the image, a rear lighting source behind the sample plane was turned on, such that lens L_5 could project the image in the sample plane onto the charge coupled device (CCD) camera.

3.2 Methods

The model has the following three main parameters; (i) the optical intensity distribution of the line pattern, (ii) the radius of a micro-sized polystyrene bead and (iii) the total power of the line pattern. Among these, the first parameter is the most complex. In this experiment, a line pattern was created by using the line optical tweezers system, as presented in Fig. 2. Next, the image processing method was used to analyze the optical intensity distribution and determine the first parameter. The other two parameters were taken directly from the known parameters that were also used in the model.

Figure 3(a) displays a partial two-dimensional image of a phase-modulated line pattern that was captured by a CCD camera with a resolution of 720×480 pixels. The image processing LabVIEW Software IMAQ was adopted to analyze the distribution of all of the gray-level values of the pixel in the image. To determine all of the gray-level values of the pixels corresponding total power P of the laser beam, the respective corresponding power P_k of the gray-level value of each pixel was determined. To simplify a two-dimensional (2D) line pattern into a one-dimensional (1D) line pattern, the power of all the longitudinal pixels that have the same coordinator as the transverse pixels was summed. Therefore, a line pattern with an equivalent 1D optical intensity distribution was evaluated and the first parameter was determined, as displayed in Fig. 3(b).

In this simulated example, the total laser power P was 100 mW; the laser wavelength λ was 1064 nm; the length of the line pattern was approximately 22.5 μm, and the total number of pixels was 278. For simplification, each pixel was treated as a trapping point, such that the total number of trapping points $m = 278$. The refraction index of the aqueous solution n_s was 1.33, and that a micro-sized polystyrene bead n_B was 1.57. Finally, a micro-sized polystyrene bead of radius r_{B1} is 3 μm, commonly adopted in experiments, were selected. The above parameters were used in the model and the trapping force distribution exerted by the line optical tweezers on the micro-sized bead was calculated.

To confirm the accuracy of the model, the actual distribution of the horizontal and vertical trapping forces exerted by the line optical tweezers on the micro-sized bead was calculated experimentally. Then, the experimental data concerning the distribution were compared with the distribution predicted by the model. The water-dragging-force and image processing methods were used to determine the trapping force distribution of the micro-sized bead that was trapped by the line optical tweezers. In the absence of flow, the attraction of the trapping force caused the micro-sized bead, close to the area of the line pattern, eventually to rest at the location in the line pattern, which was the balance point for the micro-sized bead, which the trapping force on the bead was zero. When the sample plane was moved at constant velocity by manipulating the actuator, an additional water drag force was generated, causing the bead to move toward new balance point and the trapping force was offset. Increasing the velocity of the sample plane in the horizontal

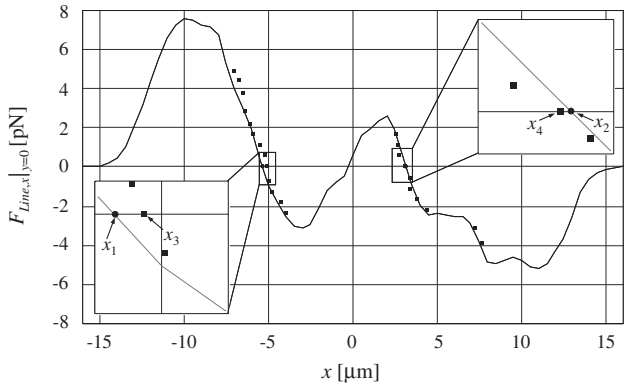

Fig. 4. Horizontal trapping force distribution for the bead of radius 3 μm. The solid curve is the model predicted value, $F_{\text{Line},x}(x)|_{y=0}$, and $x_1 = -5.37\,\mu\text{m}$ and $x_2 = 3.32\,\mu\text{m}$ are the force balance positions. The spots are the experimental data, also $x_3 = -5.14\,\mu\text{m}$ and $x_4 = 3.11\,\mu\text{m}$ are the force balance positions. The force balance positions are clear shown in the partial enlarged view.

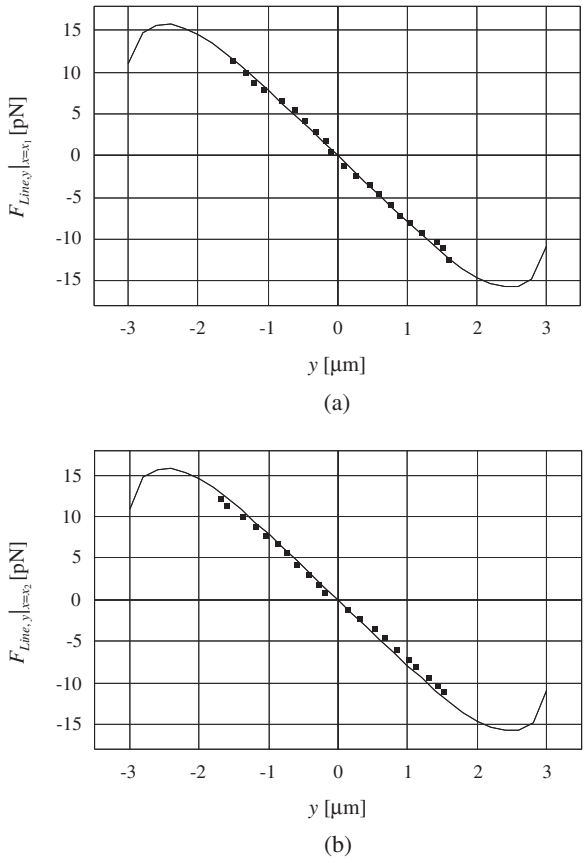

Fig. 5. The vertical trapping force distribution. (a) The force balance position is x_1; (b) the force balance position is x_2, they were easy to measure the trapping force experimentally. The solid curve was the theoretical modeling and the spots are experimental data. The errors were 1.2–10.5%.

and vertical directions of the line pattern, the micro-sized bead to move toward the new balance points until it escaped from the line trap, as observed on the video-recording. Next, an image processing method was used to locate the new balance points of each micro-sized bead for each water flow velocity. According to eq. (20), not only the water dragging force was measured but also the trapping force values were obtained in real time. Accordingly, a relationship between trapping force and the position of the micro-sized bead was demonstrated. To test the accuracy of the model, the result was compared with the predicted trapping force distribution. Finally, numerical simulation was used to calculate the trajectory and separation between the two micro-sized beads of different sizes as they flowed into the line pattern. Changing the included angle θ_w for the single water flow velocity v_w enabled each separation distance $\Delta d = d_1 - d_2$ between the two micro-sized beads up to the maximum $\Delta d_{\max}$ to be determined.

4. Results

The results of this experimental study demonstrated that the line trap model had been successfully tested. Figure 4 plots the horizontal trapping force distribution in the trapped micro-sized bead with a radius of 3 μm in the line pattern. The left and right of Fig. 4 is a partial enlarged view which shows the force balance positions. The solid curve represents the values $F_{\text{Line},x}(x)|_{y=0}$ predicted by the model, while the spots represent the experimental data. The experimental data are close to the predicted values with errors of between 0.9 and 7.1%. The predicted and experimental result also include two force balance positions ($x|_{F_{\text{Line},x}=0}$) of the trapped micro-sized bead in the identical line pattern [Fig. 3(a)]. These two positions were $x_1 = -5.37\,\mu\text{m}$ and $x_2 = 3.32\,\mu\text{m}$ (predicted), and $x_3 = -5.14\,\mu\text{m}$ and $x_4 = 3.11\,\mu\text{m}$ (experimental). Since the force balance positions were the locations where the line optical tweezers most easily trapped the micro-sized beads, the vertical trapping force distributions, $F_{\text{Line},y}(y)|_{x=x_1}$ and $F_{\text{Line},y}(y)|_{x=x_2}$, on the y-axis, shown in Figs. 5(a) and 5(b), were obtained. The experimental data are close to the predicted values with errors of between 1.2% and 10.5%. Both figures clearly indicate that the theoretical modeling (solid cure) was consistent with the experimental results (spots). Therefore, the accuracy of this model was quantitatively examined.

Then, the above results were applied to simulate the trajectory of the two known micro-sized beads as they passed through the line pattern. The trajectory is analyzed to determine the separation distance between the micro-sized beads. Based on the trajectories, Fig. 6 presents the separation distance Δd under water flow velocity $v_w = 250\,\mu\text{m/s}$; the total laser power P was 100 mW, and included angle θ_w from 0 to 80°. As the included angle θ_w increased from 0 to 45°, the separation did not increase significantly. However, as the included angle increased further, the separation distance Δd increased rapidly. The angle of 49°, $\Delta d > 6.0\,\mu\text{m}$, was the threshold included angle $\theta_{\text{w-th}}$ for the effective separation between the large bead from the small bead. It is defined as the separation distance exceeds the diameter of the large bead. It is easy to separate large bead from small bead. The maximum separation distance, $\Delta d_{\max} \cong 11.83\,\mu\text{m}$, between the two micro-sized beads was reached when the included angle was 64°. Therefore, 64° is the optimal included angle of separation. As the included angles increased beyond this value, the separation distance began to decrease gradually. The gray area of Fig. 6 is a domain of effective separation and the included angle form 49 to 80°. The left of Fig. 6 is a diagram which shows the

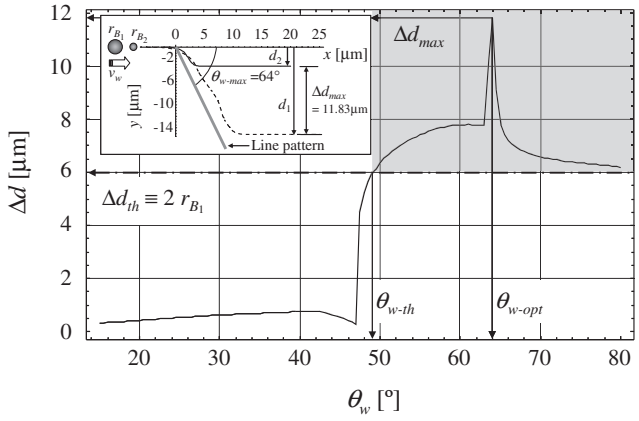

Fig. 6. The separation distance Δd under water flow velocity $v_w = 250\,\mu m/s$; the total laser power P was 100 mW: The included angle ≥49°, the separation distance Δd exceeds the diameter of the large bead, is threshold included angle. The included angle is 64°, the maximum separation distance is 11.83 μm. The gray area is a domain of effective separation. The left is a diagram which shows the relationship between trajectory and separation distance. The separation distance $\Delta d = d_1 - d_2$.

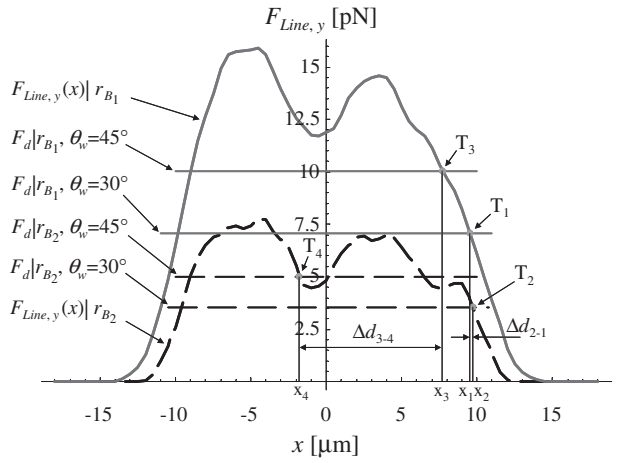

Fig. 7. Compare trapping force (curve) with water dragging force (line), understanding the effective separation. The $T_{i|i=1-4}$ is trapping force (dashed curve) less than water dragging force (dashed line), the beads escaped from these position. When the include angle θ_w is 30°, the beads moved along, and did not escape until the end of the line pattern. The large and small beads escaped from T_1 and T_2 respectively. The separation distance $\Delta d_{2\text{-}1}$ was $x_2 - x_1$. The include angle θ_w is 45°, the large and small beads escaped from T_3 and T_4 respectively. The separation distance $\Delta d_{3\text{-}4}$ was $x_3 - x_4$. Compare the separation distance, a clear separation in the included angle 45°. Accordingly, when the line pattern reaches a specific (threshold) included angle, a difference exists the effective separations between the micro-sized beads.

relationship between trajectory and separation distance. The two known micro-sized beads followed the same start and moved to the line pattern. The dashed curve represents the trajectory of the large bead r_{B1} with a radius of 3 μm and the solid curve represents that of the small bead r_{B2} with a radius of 1.5 μm. The d_1 and d_2 were vertical distances of oblique displacement in the trajectory. The difference between d_1 and d_2 was separation distance. The separation distance corresponds to the included angle. The optimal separation distance was as an example, the others were identical method of the numerical simulation.

5. Discussion

In the process of beads separation, this line pattern has a threshold included angle of effective separation $\theta_{w\text{-}th}$ and an included angle of maximum separation $\theta_{w\text{-}opt}$, clearly presented in Fig. 6. The trapping force and the water dragging force were compared to determine a threshold included angle of effective separation. To take an example, as presented in Fig. 7, both the trapping force and the water dragging force were calculated and perpendicular to the direction of the line pattern. The solid curve ($F_{\text{Line},y}(x)|r_{B_1}$) and the dashed curve ($F_{\text{Line},y}(x)|r_{B_2}$) represent the maximum trapping force distribution for the large (r_{B_1}) and small (r_{B_2}) beads, respectively, whereas the solid line ($F_d|r_{B_1}$, $\theta_w = 30$ and 45°) and the dashed line ($F_d|r_{B_2}$, $\theta_w = 30$ and 45°) represent the water dragging force, for the same water flow velocity and included angles of 30 and 45°, on the large and small beads in the line pattern. When the included angle of the line pattern is 30°, the trapping force on the two beads in the linear trapping scope exceeds the water dragging force. Consequently, both beads moved along, and did not escape until the end of the line pattern (T_1 and T_2). The separation distance, $\Delta d_{2\text{-}1} = x_2 - x_1$, was small. When the included angle in the line pattern became 45°, the trapping force is less than the water dragging force at T_3 in Fig. 7, the small bead could no longer resist the water dragging force and escaped from the line pattern. However, at the same included angle of 45°, the trapping force still exceeded the water dragging force, the large bead remained on the line pattern until it was beyond the influence of the trapping force (T_4). The separation distance, $\Delta d_{3\text{-}4} = x_3 - x_4$, was large. Based on the separation distance, the included angle of 45° can be used to distinguish the large from the small bead. Therefore, the water dragging force and the distribution of the trapping forces of the line pattern at different included angle affects the separation between the micro-sized beads. Additionally, when the line pattern reaches a specific (threshold) included angle at a given water flowing velocity, a difference exists the effective separations between the micro-sized beads, as shown in Fig. 6.

The simulation and the experimental results show that the optical intensity distribution of the line pattern determines not only the distribution of the trapping force but the trajectory and the separation between the micro-sized beads. Therefore, designing a line pattern with suitable intensity could help effectively to extend the optimum separation conditions. Then, this scheme may be applied to biological and medical detections.

6. Conclusions

This study presented the line optical tweezers system, and a model thereof, and simulates the separation between differently micro-sized beads to determine separation condition. According to the model, four main factors determine the separation: optical intensity distribution of a line pattern, radius of micro-sized beads, flow velocity and included angle. A comparison the measurements of force verified that the model was precise to predict the trapping force of the trapped micro-size beads in the line optical trapping. The

model and the equation of motion were used to simulate the trajectory of differently sized micro-sized beads on the line pattern and to determine optimal and effective separation. Therefore, the simulation calculations support the design and manipulation of the line optical trapping.

For practical applications, a microchannel chip based on simulated parameters was designed by modeling a simulated sample that was both before and after testing. Combining the line optical tweezers with a designed microchannel chip will enable a fast, precise, and effective sorting and screening method for the chip to be implemented, supporting further quantitative analysis. Restated, this study has provided a novel biological detection method and a powerful tool in the miniaturization of cells/beads separation techniques.

Acknowledgements

The authors would like to thank the National Science Council of the Republic of China, Taiwan, for financially supporting this research under Contract No. NSC96-2120-M-009-003. Ted Knoy is appreciated for his editorial assistance.

1) A. Ashkin, J. M. Dziedzic, J. E. Bjorkholm, and S. Chu: Opt. Lett. **11** (1986) 288.
2) A. Ashkin and J. M. Dziedzic: Science **235** (1987) 1517.
3) S. C. Grover, A. G. Skirtach, R. C. Gauthier, and C. P. Grover: J. Biomed. Opt. **6** (2001) 14.
4) Y. Wakamoto, I. Inoue, H. Moriguchi, and K. Yasuda: Fresen. J. Anal. Chem. **371** (2001) 276.
5) M. Ozkan, M. Wang, C. Ozkan, R. Flynn, A. Birkbeck, and S. Esener: Biomed. Microdevices **5** (2003) 61.
6) M. Ozkan, T. Pisanic, J. Scheel, C. Barlow, S. Esener, and S. N. Bhatia: Langmuir **19** (2003) 1532.
7) A. D. Mehta, M. Rief, J. A. Spudich, D. A. Smith, and R. M. Simmons: Science **283** (1999) 1689.
8) M. Reicherter, T. Haist, E. U. Wagemann, and H. J. Tiziani: Opt. Lett. **24** (1999) 608.
9) J. Liesener, M. Reicherter, T. Haist, and H. J. Tiziani: Opt. Commun. **185** (2000) 77.
10) J. E. Curtis, B. A. Koss, and D. G. Grier: Opt. Commum. **207** (2002) 169.
11) S. Tseng, S. Chi, and L. Hsu: Proc. SPIE **5514** (2004) 687.
12) Y. Roichman and D. G. Grier: Opt. Lett. **31** (2006) 1675.
13) Y. Roichman, I. Cholis, and D. G. Grier: Opt. Express **14** (2006) 10907.
14) A. Ashkin: Phys. Rev. Lett. **24** (1970) 156.
15) A. Ashkin: Biophys. J. **61** (1992) 569.
16) K. S. Yee: IEEE Trans. Antennas Propag. **14** (1966) 302.